Editors' Suggestion   Featured in Physics

Hamiltonian Ratchet for Matter-Wave Transport

N. Dupont [1,2] L. Gabardos,[1] F. Arrouas,[1] N. Ombredane,[1] J. Billy,[1] B. Peaudecerf,[1] and D. Guéry-Odelin[1]

[1]*Laboratoire Collisions Agrégats Réactivité, UMR 5589, FERMI, UT3, Université de Toulouse, CNRS,*
118 Route de Narbonne, 31062 Toulouse CEDEX 09, France
[2]*Center for Nonlinear Phenomena and Complex Systems, Université Libre de Bruxelles,*
CP 231, Campus Plaine, B-1050 Brussels, Belgium

We report on the design of a Hamiltonian ratchet exploiting periodically at rest integrable trajectories in the phase space of a modulated periodic potential, leading to the linear nondiffusive transport of particles. Using Bose-Einstein condensates in a modulated one-dimensional optical lattice, we make the first observations of this spatial ratchet, which provides way to coherently transport matter waves with possible applications in quantum technologies. In the semiclassical regime, the quantum transport strongly depends on the effective Planck constant due to Floquet state mixing. We also demonstrate the interest of quantum optimal control for efficient initial state preparation into the transporting Floquet states to enhance the transport periodicity.

The ratchet effect is the well-known yet intriguing phenomenon which sees the emergence of a directed current for particles initially at rest in a space and time periodic modulated potential, while no net average force is exerted on the system. Its origin is well understood and relies minimally on the breaking of space and time reversal symmetries [1–3]. Two main families of ratchets can be distinguished: on one hand, *Brownian ratchets* are systems experiencing stochastic forces, where the potential rectifies the isotropy of Brownian motion [4] into a net directed transport [5–11]. Such ratchets are thought to take part in the operation of molecular motors [12,13], as for instance in the case of kinesin [14]. They are usually studied in the overdamped regime to model the strong dissipation of biological media [11,15]. On the other hand, *deterministic ratchets*, which can be either dissipative [1,16–19] or Hamiltonian (see below), are systems for which the classical dynamics is well captured by their phase-space flow. Such Hamiltonian systems, under moderate temporal driving, exhibit a mixed dynamics with phase portraits displaying islands of regular trajectories embedded in a chaotic sea of nonintegrable ones (see, e.g., Fig. 1).

Studies on Hamiltonian ratchets have mainly focused thus far on delocalized transport configurations, where the directed transport originates either in a momentum-asymmetric chaotic sea (in the classical case from trajectories ergodically spanning the chaotic sea [1,8,20], and in the quantum case through state coupling with eigenstates delocalized over it [20–23]), or by resonantly accelerating particles in the case of quantum-resonance ratchets [24,25]. In contrast, Hamiltonian ratchets relying on regular islands of quasiperiodic trajectories offer a mean to incrementally transport localized particles on a periodic substrate in a

ballistic way [21]. Note that this transport appears classically and is distinct from topological pumping effects (Ref. [26] and references therein). Such regular Hamiltonian ratchets have been experimentally studied mainly with phase-shifted kicked rotors, implemented in cold atom systems, in the case of stepwise transport along the momentum direction (an *accelerator ratchet*) [27–30], and with only up to 20% of an initial atom packet loaded in the transporting island. Meanwhile, regular Hamiltonian
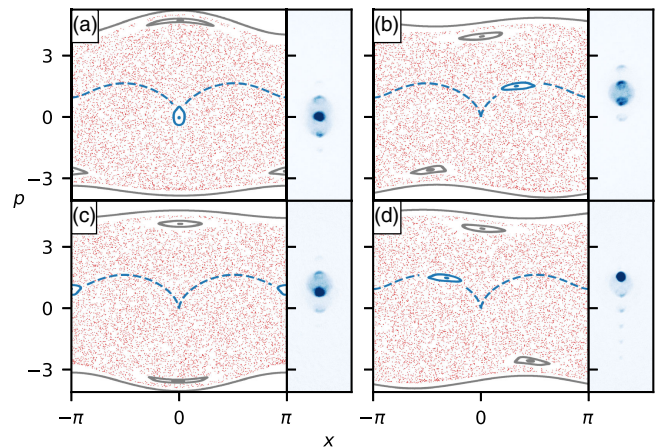

FIG. 1. Stroboscopic phase portraits and experimental images for $(\gamma, \varepsilon, \varphi_0) = (1.2, 0.3, 1.7)$ at subperiod observation times $t = (n + r) \times 2\pi$ [with $n \in \mathbb{N}$ and $r = 0$, 0.25, 0.5, and 0.75 for (a) to (d) respectively]. Left: the ratcheting island and the trajectory starting in $(x_0, p_0, t_0) = (0, 0, 0)$ are in blue, the other regular structures are in gray, and the chaotic sea is in red. The area of the ratcheting island is $\mathcal{A} = 0.21$. Right: corresponding time-of-flight absorption images, starting from the ground state of the lattice during the first period $n = 0$ for $1/\hbar_{\text{eff}} \approx 1.27$.

ratchets along the position coordinate [31] remain unexplored experimentally so far. Beyond the use of regular islands with a ballistic motion at all times, as found, e.g., in the kicked rotor, of particular interest is the design of a dynamical system in which the transporting island periodically coincides with the ground state of the potential, in which a collection of particles initially at rest can therefore be directly loaded and transported.

In this Letter, we solve this nontrivial problem, the solution of which we refer to as a *spatial halting ratchet* (SHR). We show how such a solution can be engineered with a simple gating ratchet [32,33], a one-dimensional space-symmetric potential modulated in amplitude and phase. We obtain parameters leading to classical orbits of initial zero velocity having a ratcheting motion of one spatial period per modulation period. For these parameters, we study quantum transport as a function of the effective reduced Planck constant $\hbar_{\text{eff}}$, a free quantum parameter that sets the minimal phase-space area of quantum states without altering the classical dynamics. As a modulation parameter (e.g., $\hbar_{\text{eff}}$) is varied, avoided crossings in the Floquet spectrum lead to state mixing. Although this phenomenon is sought after in the case of diffusive Hamiltonian ratchets [22,34] where it is the source of transport, and is also key in chaos-assisted tunneling [35,36], it has a deleterious effect in the regular transport case, as a wave packet initially prepared over the classical ratcheting island may dynamically tunnel [37] out of it. This may be avoided by a precise choice of parameter values, or controlled through specific state preparation. From our theoretical analysis, we implement and observe experimentally the SHR with matter waves, using Bose-Einstein condensates (BECs) in a modulated one-dimensional optical lattice. We first perform these experiments by loading the ratcheting Floquet state from the ground state of the lattice. For values of $\hbar_{\text{eff}}$ for which the ratcheting island is substantially coupled with the chaotic sea, we then show how one can account for state mixing by employing quantum optimal control (QOC) [38,39] to optimize the loading of the proper Floquet state.

Classical dynamics.—We consider the case of an inertial particle in a gating potential [32,33]. Its dynamics is governed by the dimensionless Hamiltonian

$$H(x, p, t) = \frac{p^2}{2} - \gamma[1 + \varepsilon \cos(t)] \cos [x - \varphi_0 \sin(t)]. \quad (1)$$

The Hamiltonian of Eq. (1), with its 1:1 frequency ratio and phase quadrature between amplitude and phase modulations, breaks the relevant space and time symmetries [1,33], leading to a momentum-asymmetric chaotic sea carrying diffusive ratchet transport. In contrast, the dimensionless modulation parameters $(\gamma, \varepsilon, \varphi_0)$ can also be chosen so that a transporting regular region emerges in the center of the chaotic sea, i.e., such that a bundle of

trajectories starting around $(x_0, p_0) = (0, 0)$ at $t_0 = 0$ goes to the neighborhood of $(x_0 + 2\pi, p_0)$ at $t = 2\pi$. We achieve this numerically by minimizing with respect to $(\gamma, \varepsilon, \varphi_0)$ (using a Nelder-Mead algorithm) the total variation of mechanical energy over one modulation period for a set of trajectories that start near (x_0, p_0) and change site. This yields several solutions [40]. In the following we use $(\gamma, \varepsilon, \varphi_0) = (1.2, 0.3, 1.7)$, a set of parameters that generates a SHR with the ratcheting island seen in the stroboscopic phase portraits of Fig. 1.

Quantum ratchet in a regular island.—The natural basis to stroboscopically study quantum dynamics in a time-periodic potential is the set of Floquet states, the eigenstates of the evolution operator over one period of modulation. The quantum study leaves as a free parameter the effective reduced Planck constant $\hbar_{\text{eff}} = -i[\hat{x}, \hat{p}]$ that dictates the minimal phase-space area $\Delta x \Delta p$ of quantum states in the system. As we are interested in the transport of a quantum particle on the ratcheting island, we place our study at the onset of the semiclassical regime, that is for $\hbar_{\text{eff}} \sim \mathcal{A}$, with $\mathcal{A}$ the area of the studied regular structures in phase space (Fig. 1). In the semiclassical regime, Floquet states are generally either localized on regular islands or spread over the chaotic sea [41,42], with only one state per island for $\hbar_{\text{eff}} \sim \mathcal{A}$. The quantum analog of the periodic classical trajectories at the center of the stroboscopic phase portraits of Fig. 1(a) is therefore the Floquet state $|F_{\text{rat}}\rangle$ that can be associated with the ratcheting island. This state is identified from its overlap with the ground state $|\phi_0\rangle$ of the static lattice potential [that is $\varepsilon = 0$ and $\varphi_0 = 0$ in Eq. (1); a state readily accessible in the experiment]. Furthermore, we define the expected transport of a state $|\psi(t_0)\rangle$ between the times t_0 and t_1 as

$$\Delta x_{(t_0, t_1)}(\psi) = \int_{t_0}^{t_1} \langle \hat{p} \rangle_{\psi(t)} dt. \quad (2)$$

The transport over one period $\Delta x_{(0, 2\pi)}(F)$ for a Floquet state $|F\rangle$ is related to its time-averaged group velocity $\bar{v}_g$ in the Floquet spectrum, $\Delta x_{(0, 2\pi)}(F) = 2\pi \bar{v}_g$ (see Supplemental Material [43]). In the semiclassical regime, one expects regular Floquet states to behave as their associated region of regular classical trajectories, and, in particular for the ratcheting Floquet state, $\Delta x_{(0, 2\pi)}(F_{\text{rat}}) \approx 2\pi$. Therefore in that regime, the very existence of a transporting regular island generally guarantees for all quasimomenta (see below and Supplemental Material [43]) the existence of a localized transporting Floquet state, a key feature differing from previous ballistic ratchets [22,23].

We illustrate these notions in Fig. 2 where numerical results for the transport of noninteracting wave functions in the ratcheting island as a function of $1/\hbar_{\text{eff}}$ are shown. Figure 2(a) shows the overlap between $|F_{\text{rat}}\rangle$ and the ground state $|\phi_0\rangle$. This metric informs on the phase-space centering of $|F_{\text{rat}}\rangle$, as well as on its expected loading when running the
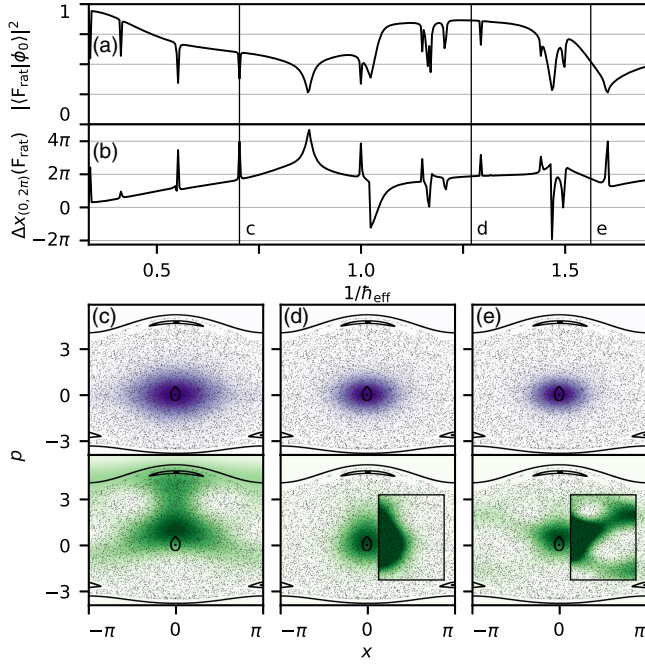
FIG. 2. Eigenstate and transport dependences on the effective Planck constant. (a) Overlap between the ground state $|\phi_0\rangle$ of the lattice and the ratcheting Floquet state $|F_{\text{rat}}\rangle$ and (b) transport [Eq. (2)] of $|F_{\text{rat}}\rangle$ over one modulation period as a function of $1/\hbar_{\text{eff}}$. (c)–(e) Stroboscopic phase portraits in the unit cell of system [Eq. (1)] and Husimi representations of $|\phi_0\rangle$ (top, purple) and $|F_{\text{rat}}\rangle$ (bottom, green) for the values of $1/\hbar_{\text{eff}} = 0.70$, 1.27, 1.56 respectively, identified by vertical lines on the panels (a)–(b). The color range for each Husimi function extends from zero to its maximum value, with a truncation to a quarter of this value in the outlined rectangular regions of panels (d) and (e) in order to reveal details (note that the Floquet states share the $x \rightarrow -x$ symmetry of the phase portrait).

experiment with $|\phi_0\rangle$ as the initial state. Figure 2(b) shows the expected periodic transport of $|F_{\text{rat}}\rangle$. As $1/\hbar_{\text{eff}}$ varies, both $|\langle\phi_0|F_{\text{rat}}\rangle|^2$ and $\Delta x_{(0,2\pi)}(F_{\text{rat}})$ [Figs. 2(a) and 2(b) respectively] display sharp nonmonotonic fluctuations ascribed to Floquet state mixing: the variation of quasienergy levels in the Floquet spectrum gives rise to avoided crossings leading to sharp changes of the Floquet states near the crossings (see Supplemental Material [43]).

Figures 2(c)–2(e) show the Husimi quasidistributions of $|\phi_0\rangle$ and $|F_{\text{rat}}\rangle$ for different values of $1/\hbar_{\text{eff}}$. At given coordinates (x, p), this phase space representation of a quantum state corresponds to the evaluation of its overlap with a Gaussian state centered in (x, p) [44,45]. With $1/\hbar_{\text{eff}} = 1.27$, Fig. 2(d) is an example of a semiclassical, island-shaped $|F_{\text{rat}}\rangle$, with a ground state overlap $|\langle\phi_0|F_{\text{rat}}\rangle|^2 = 0.86$ and a periodic transport $\Delta x_{(0,2\pi)}(F_{\text{rat}}) = 0.93 \times 2\pi$, meaning that this state exhibits a stationary flux of particles, periodically at rest at the bottom of the lattice wells. On the other hand, Figs. 2(c) and 2(e) correspond to respectively smaller and larger values of $1/\hbar_{\text{eff}}$ for which the system initialized in $|\phi_0\rangle$ evolves out of

it [toward a mode of high momentum for Fig. 2(c) and over the chaotic sea for Fig. 2(e)]. Figure 2 shows overall that, for sufficiently large values of $1/\hbar_{\text{eff}}$ and while paying attention to Floquet state mixing, a SHR with a semiclassical periodic transport of quantum states can be achieved, with $\Delta x_{(0,2\pi)}(F_{\text{rat}})$ fluctuating around 2π for $1/\hbar_{\text{eff}} > 0.75$.

Ratchet transport from the ground state.—We experimentally observe a SHR with matter waves using BECs of 5×10^5 ^{87}Rb atoms initially obtained in a hybrid trap setup [46]. The atoms are adiabatically loaded at time $T_0 = 0$ in the ground state $|\phi_0\rangle$ of the optical lattice potential

$$V(X, T) = -A(T)\frac{s}{2}E_L\cos\left(\frac{2\pi X}{d} + \varphi(T)\right), \quad (3)$$

with $A(T_0) = 1$ and $\varphi(T_0) = 0$ (we denote with capital X, P, and T dimensional quantities). The optical lattice is produced by the superposition of two counterpropagating far-detuned laser beams of wavelength $\lambda = 1064$ nm. Before each experiment, we independently calibrate [47] the depth s of the lattice in units of the lattice energy scale $E_L = h^2/2md^2$ (with $d = \lambda/2$ the lattice spacing, m the atomic mass and h Planck's constant). The driving amplitude of an acousto-optic modulator (AOM) placed before the splitting of the lattice beams controls $A(T)$, while the relative driving phase of two AOMs placed on each beam after the splitting controls $\varphi(T)$. The optical lattice potential [Eq. (3)], with the correlated modulation functions $A(T) = [1 + \varepsilon\cos(\omega T)]$ and $\varphi(T) = -\varphi_0\sin(\omega T)$ where ω is the modulation angular frequency, yields the dimensionless gating Hamiltonian [Eq. (1)] for $\gamma = s(E_L/\hbar\omega)^2$ and an effective reduced Planck constant $\hbar_{\text{eff}} = 2E_L/\hbar\omega$ [48].

The $1/\hbar_{\text{eff}}$ range of Fig. 2 corresponds in practice to a lattice depth range $s \in [0.5, 14]$. A weak harmonic trapping with angular frequencies $(\Omega_X, \Omega_Y, \Omega_Z) = 2\pi \times (10.4, 66, 68)$ Hz remains present during experiments, but its impact is negligible over the short experimental times of up to ~ 500 µs in this Letter. In the subspace of null quasimomentum, the BEC state along the x axis is thus described by a superposition of plane waves

$$|\psi(T)\rangle = \sum_{\ell \in \mathbb{Z}} c_\ell(T)|\chi_\ell\rangle, \quad (4)$$

with the coefficients $c_\ell(T) \in \mathbb{C}$, $\sum_\ell |c_\ell(T)|^2 = 1$, and $\langle X|\chi_\ell\rangle = e^{i\ell k_L X}/\sqrt{d}$, where $k_L = 2\pi/d$ is the lattice wave vector. Finally, we access at time T the BEC momentum distribution by absorption imaging following a 35 ms time of flight. We obtain the typical diffraction patterns of Fig. 1, from which we extract $|c_\ell(T)|^2$. The experimental transport [Eq. (2)] is then computed by sampling the average momentum $\langle\hat{P}\rangle_{\psi(T)}/\hbar k_L = \sum_\ell \ell|c_\ell(T)|^2$ in the course of the ratchet modulation. In this system, a transport of one site per modulation period corresponds to a velocity $v = \hbar k_L/m\hbar_{\text{eff}} \approx 8.63/\hbar_{\text{eff}}$ mm/s.
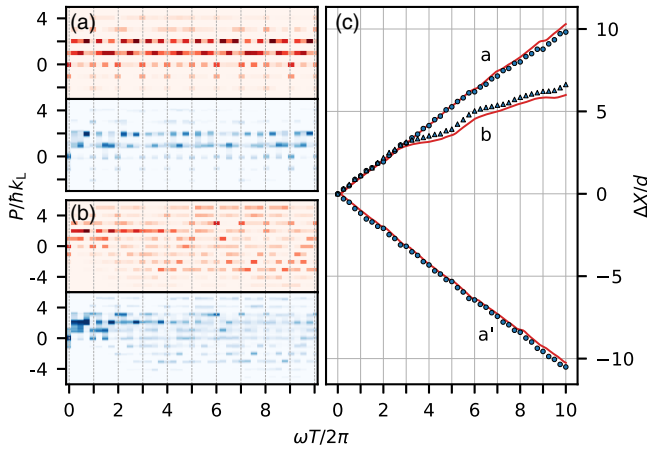
FIG. 3. Transport of the ground state. (a) Top: numerical simulation of the momentum distribution during the modulation as a function of time for $1/\hbar_{\mathrm{eff}} \approx 1.27$ [corresponding to Fig. 2(d)]. Bottom: corresponding experimental integrated absorption images. (b) Same as (a) for $1/\hbar_{\mathrm{eff}} \approx 1.56$ [corresponding to Fig. 2(e)]. (c) Expected numerical (solid red line) and experimental (blue markers) transport (see text) for data (a) and (b) as a function of time, and transport reversability (a') for $\varphi_0 \rightarrow -\varphi_0$ and $1/\hbar_{\mathrm{eff}} \approx 1.30$ (see text).

We first perform ratchet transport experiments with $|\phi_0\rangle$ as the initial state. We acquire four images per modulation period over ten periods (as shown in Fig. 1 for the first period). Figure 3 shows, for two values of $1/\hbar_{\mathrm{eff}}$, the experimental evolution of the momentum distribution and the resulting integrated transport compared with numerical simulations of the same quantities from the integration of the Schrödinger equation. The values of $1/\hbar_{\mathrm{eff}}$ in Figs. 3(a) and 3(b) correspond to those of Figs. 2(d) and 2(e) respectively. For Fig. 3(a), $|\phi_0\rangle$ is rather well projected onto $|F_{\mathrm{rat}}\rangle$ [Figs. 2(a) and 2(d)]. We thus observe an almost periodic evolution of the momentum distribution, mainly carried by plane waves of positive momentum and resulting in a linear semiclassical ratchet transport over ten lattice sites in ten modulation periods [Fig. 3(c); a study of the transport over longer timescales is detailed in the Supplemental Material [43]). In the experiment of Fig. 3(b) however, as $|\phi_0\rangle$ has limited overlap with $|F_{\mathrm{rat}}\rangle$, which moreover extends over the chaotic sea [Fig. 2(e)], we observe a nonperiodic evolution of the momentum distribution associated with a diffusion over the chaotic sea as seen from the increase of the momentum dispersion. This results in a nonlinear evolution of the transport [Fig. 3(c)], in contrast to its classical counterpart. Interestingly, this nonclassical behavior happens for a smaller value of $\hbar_{\mathrm{eff}}$, highlighting the quantum nature of the underlying mechanism of state mixing.

A key feature of the ratchet effect is the ability to reverse the transport direction via adequate symmetries [3,11]. In our gating system, this transport direction is imposed by the sign of the phase quadrature between the amplitude

and phase modulations [Eq. (1)]. The change $\varphi(t) = -\varphi_0 \sin(t) \rightarrow +\varphi_0 \sin(t)$ is thus expected to result in a reversed ratchet transport in the lattice. In Fig. 3(c), the integrated transport for $(\gamma, \varepsilon, \varphi_0) = (1.2, 0.3, -1.7)$ and a value of $\hbar_{\mathrm{eff}}$ similar to that of panel (a) is shown [with label (a')]. We measure as expected a symmetric ratchet transport over -10 sites in ten modulation periods. We get an overall excellent agreement between experiments and simulations.

*Optimized loading through quantum optimal control.—*Even for values of $1/\hbar_{\mathrm{eff}}$ for which $\Delta x_{(0,2\pi)}(F_{\mathrm{rat}}) \approx 2\pi$, semiclassical ratchet transport can be limited when working with $|\phi_0\rangle$ as the initial state [see, e.g., Figs. 2(a), 2(b), and 2(e)]. To enhance this transport, we use, in a second set of experiments, the phase of the lattice φ as a control parameter to optimally prepare $|F_{\mathrm{rat}}\rangle$ before applying the ratchet modulation. To that end, after determination of $|F_{\mathrm{rat}}\rangle$, an optimal phase variation $\varphi(0 < T < T_c)$ in the lattice of fixed depth s is computed using a first-order gradient-ascent algorithm (detailed with its experimental implementation in previous works [45,49]), to drive the BEC from $|\phi_0\rangle$ to $|F_{\mathrm{rat}}\rangle$. We set in this Letter $T_c \approx 80$ μs. The QOC algorithm converges to a control field that theoretically prepares a state $|\psi_{\mathrm{QOC}}\rangle$ with a fidelity of $|\langle F_{\mathrm{rat}}|\psi_{\mathrm{QOC}}\rangle|^2 \geq 0.995$ [50], while the fidelities experimentally reached for such targets are typically ~ 0.95 [45]. We illustrate in Figs. 4(a)–4(c) the QOC
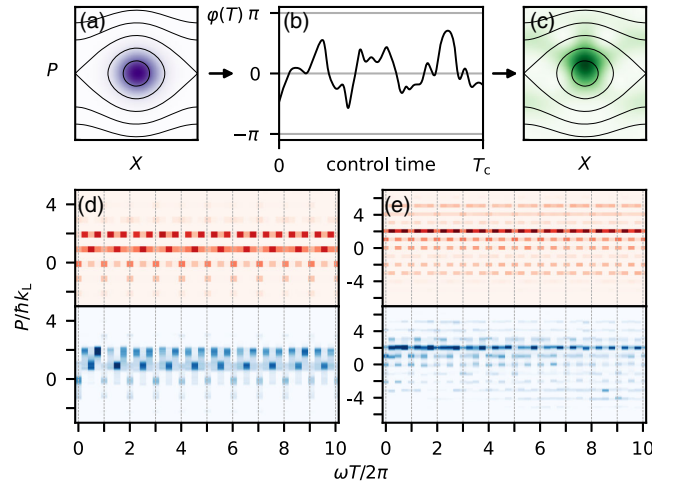

FIG. 4. Transport of the ratcheting Floquet state prepared by QOC. (a)–(c) Example of QOC for ratchet transport at $1/\hbar_{\mathrm{eff}} \approx 1.56$. (a) Husimi representation of $|\phi_0\rangle$ (purple) in the phase space of the static lattice (solid black lines). The color range for the Husimi function extends from zero to its maximum value. (b) Phase of the lattice along time to drive the system from $|\phi_0\rangle$ to $|F_{\mathrm{rat}}\rangle$. (c) Same as (a) for the prepared state $|\psi_{\mathrm{QOC}}\rangle$. (d) Top: numerical simulation of the momentum distribution during the modulation as a function of time for $1/\hbar_{\mathrm{eff}} \approx 1.27$ [corresponding to Figs. 2(d) and 3(a)]. Bottom: corresponding experimental integrated absorption images. (e) Same as (d) for $1/\hbar_{\mathrm{eff}} \approx 1.56$ [corresponding to panels (a)–(c) as well as Figs. 2(e) and 3(b)].

protocol of Floquet state preparation, with an optimized $\varphi(T)$ driving $|\phi_0\rangle$ to $|F_{\text{rat}}\rangle$ for a given value of $1/\hbar_{\text{eff}}$ [corresponding to Figs. 2(e) and 3(b)]. Figures 4(d) and 4(e) show experimental results and numerical simulations for the same parameters as Figs. 3(a) and 3(b) respectively, with a preliminary QOC preparation applied. While the experiment of Fig. 3(a) already featured a clear linear quantum transport, Fig. 4(d) demonstrates how the QOC preparation of the ratcheting Floquet state enhances the periodicity of the momentum evolution. Comparing Fig. 4(e) with Fig. 3(b), the gain is even more spectacular. Interestingly, Fig. 4(e) displays a broad momentum dispersion from the beginning of the modulation, which demonstrates the preparation of a ratcheting Floquet state partially extending over the chaotic sea as expected [see Fig. 2(e)].

Conclusion.—In this Letter, we have studied a spatial Hamiltonian ratchet effect exploiting regular trajectories in phase space to transport particles periodically at rest. We showed how such a SHR can be obtained classically within a gating ratchet. We then considered quantum transport in the near semiclassical regime, for small but realistic values of the effective Planck constant $\hbar_{\text{eff}}$, and discussed how quantum transport can be strongly affected by Floquet state mixing as $\hbar_{\text{eff}}$ varies. We experimentally observed coherent SHR transport of matter waves with BECs of ^{87}Rb in a modulated optical lattice. For values of $\hbar_{\text{eff}}$ coupling the ratcheting island with the chaotic sea, we witnessed how atoms loaded in the island evolve out of it through dynamical tunneling. Finally, we demonstrated how this effect can be mitigated through the use of state control methods such as QOC, to prepare the ratcheting Floquet state and thus enhance the periodicity of the dynamics.

Our modeling relies on an infinite lattice description, and is in good agreement with experimental data. Finite-size effects therefore have a limited impact on our experiments, which is due both to the extension of the BEC (≈ 100 lattice sites) and to the fact that in the cases studied here the ratcheting Floquet state has a uniform group velocity in the vicinity of zero quasimomentum (see Supplemental Material [43]).

The regular ratchet effect we demonstrated constitutes a novel way to coherently transport matter waves in a periodic potential, alongside conveyor belt approaches [51–53]. Higher SHR currents could be obtained by decreasing $\hbar_{\text{eff}}$ in a deeper lattice. Our results lend themselves to further investigations, such as the extension to higher dimensional modulated lattices, the investigation of the impact of interactions on the transport dynamics, or the use of optimal control to optimize the actual shape of the transporting state, in order, e.g., to maximize its initial overlap with the ground state of the potential.

We thank Gabriel Chatelain and Maxime Martinez for helpful discussions as well as Alexandre Dugelay for

[1] S. Flach, O. Yevtushenko, and Y. Zolotaryuk, Directed Current due to Broken Time-Space Symmetry, Phys. Rev. Lett. **84**, 2358 (2000).

[2] S. Denisov, S. Flach, A. A. Ovchinnikov, O. Yevtushenko, and Y. Zolotaryuk, Broken space-time symmetries and mechanisms of rectification of ac fields by nonlinear (non)adiabatic response, Phys. Rev. E **66**, 041104 (2002).

[3] S. Denisov, S. Flach, and P. Hänggi, Tunable transport with broken space–time symmetries, Phys. Rep. **538**, 77 (2014).

[4] P. Hänggi and F. Marchesoni, Introduction: 100 years of Brownian motion, Chaos **15**, 026101 (2005).

[5] J. Rousselet, L. Salome, A. Ajdari, and J. Prost, Directional motion of Brownian particles induced by a periodic asymmetric potential, Nature (London) **370**, 446 (1994).

[6] C. Mennerat-Robilliard, D. Lucas, S. Guibal, J. Tabosa, C. Jurczak, J.-Y. Courtois, and G. Grynberg, Ratchet for Cold Rubidium Atoms: The Asymmetric Optical Lattice, Phys. Rev. Lett. **82**, 851 (1999).

[7] R. D. Astumian and P. Hänggi, Brownian motors, Phys. Today **55**, No. 11, 33 (2002).

[8] M. Schiavoni, L. Sanchez-Palencia, F. Renzoni, and G. Grynberg, Phase Control of Directed Diffusion in a Symmetric Optical Lattice, Phys. Rev. Lett. **90**, 094101 (2003).

[9] L. Sanchez-Palencia, Directed transport of Brownian particles in a double symmetric potential, Phys. Rev. E **70**, 011102 (2004).

[10] P. Sjölund, S. J. H. Petra, C. M. Dion, S. Jonsell, M. Nylén, L. Sanchez-Palencia, and A. Kastberg, Demonstration of a Controllable Three-Dimensional Brownian Motor in Symmetric Potentials, Phys. Rev. Lett. **96**, 190602 (2006).

[11] P. Hänggi and F. Marchesoni, Artificial Brownian motors: Controlling transport on the nanoscale, Rev. Mod. Phys. **81**, 387 (2009).

[12] F. Jülicher, A. Ajdari, and J. Prost, Modeling molecular motors, Rev. Mod. Phys. **69**, 1269 (1997).

[13] D. Chowdhury, A. Schadschneider, and K. Nishinari, *Traffic phenomena in biology: From molecular motors to organisms, in Traffic and Granular Flow'05*, edited by A. Schadschneider, T. Pöschel, R. Kühne, M. Schreckenberg, and D. E. Wolf (Springer Berlin Heidelberg, Berlin, Heidelberg, 2007), pp. 223–238.

[14] M. Nishiyama, H. Higuchi, and T. Yanagida, Chemomechanical coupling of the forward and backward steps of single kinesin molecules, Nat. Cell Biol. **4**, 790 (2002).

[15] P. Reimann, Brownian motors: Noisy transport far from equilibrium, Phys. Rep. **361**, 57 (2002).

[16] P. Jung, J. G. Kissner, and P. Hänggi, Regular and Chaotic Transport in Asymmetric Periodic Potentials: Inertia Ratchets, Phys. Rev. Lett. **76**, 3436 (1996).

[17] G. G. Carlo, G. Benenti, G. Casati, and D. L. Shepelyansky, Quantum Ratchets in Dissipative Chaotic Systems, Phys. Rev. Lett. **94**, 164101 (2005).

[18] L. Wang, G. Benenti, G. Casati, and B. Li, Ratchet Effect and the Transporting Islands in the Chaotic Sea, Phys. Rev. Lett. **99**, 244101 (2007).

[19] S. Denisov, S. Kohler, and P. Hänggi, Underdamped quantum ratchets, Europhys. Lett. **85**, 40003 (2009).

[20] H. Schanz, M.-F. Otto, R. Ketzmerick, and T. Dittrich, Classical and Quantum Hamiltonian Ratchets, Phys. Rev. Lett. **87**, 070601 (2001).

[21] S. Denisov, L. Morales-Molina, S. Flach, and P. Hänggi, Periodically driven quantum ratchets: Symmetries and resonances, Phys. Rev. A **75**, 063424 (2007).

[22] T. Salger, S. Kling, T. Hecking, C. Geckeler, L. Morales-Molina, and M. Weitz, Directed transport of atoms in a Hamiltonian quantum ratchet, Science **326**, 1241 (2009).

[23] F. Zhan, S. Denisov, A. V. Ponomarev, and P. Hänggi, Quantum ratchet transport with minimal dispersion rate, Phys. Rev. A **84**, 043617 (2011).

[24] E. Lundh and M. Wallin, Ratchet Effect for Cold Atoms in an Optical Lattice, Phys. Rev. Lett. **94**, 110603 (2005).

[25] J. Ni, S. Dadras, W. K. Lam, R. K. Shrestha, M. Sadgrove, S. Wimberger, and G. S. Summy, Hamiltonian ratchets with ultra-cold atoms, Ann. Phys. (Berlin) **529**, 1600335 (2017).

[26] R. Citro and M. Aidelsburger, Thouless pumping and topology, Nat. Rev. Phys. **5**, 87 (2023).

[27] J. Gong and P. Brumer, Directed anomalous diffusion without a biased field: A ratchet accelerator, Phys. Rev. E **70**, 016202 (2004).

[28] M. Sadgrove, T. Schell, K. Nakagawa, and S. Wimberger, Engineering quantum correlations to enhance transport in cold atoms, Phys. Rev. A **87**, 013631 (2013).

[29] D. H. White, S. K. Ruddell, and M. D. Hoogerland, Experimental realization of a quantum ratchet through phase modulation, Phys. Rev. A **88**, 063603 (2013).

[30] C. Hainaut, A. Rançon, J.-F. Clément, J. C. Garreau, P. Szriftgiser, R. Chicireanu, and D. Delande, Ratchet effect in the quantum kicked rotor and its destruction by dynamical localization, Phys. Rev. A **97**, 061601(R) (2018).

[31] T. Dittrich, R. Ketzmerick, M.-F. Otto, and H. Schanz, Classical and quantum transport in deterministic Hamiltonian ratchets, Ann. Phys. (Berlin) **512**, 755 (2000).

[32] M. Borromeo and F. Marchesoni, Noise-assisted transport on symmetric periodic substrates, Chaos **15**, 026110 (2005).

[33] R. Gommers, V. Lebedev, M. Brown, and F. Renzoni, Gating Ratchet for Cold Atoms, Phys. Rev. Lett. **100**, 040603 (2008).

[34] C. Grossert, M. Leder, S. Denisov, P. Hänggi, and M. Weitz, Experimental control of transport resonances in a coherent quantum rocking ratchet, Nat. Commun. **7**, 10440 (2016).

[35] S. Tomsovic and D. Ullmo, Chaos-assisted tunneling, Phys. Rev. E **50**, 145 (1994).

[36] M. Arnal, G. Chatelain, M. Martinez, N. Dupont, O. Giraud, D. Ullmo, B. Georgeot, G. Lemarié, J. Billy, and D. Guéry-Odelin, Chaos-assisted tunneling resonances in a synthetic Floquet superlattice, Sci. Adv. **6**, eabc4886 (2020).

[37] *Dynamical Tunneling: Theory and Experiment*, edited by S. Keshavamurthy and P. Schlageck (CRC Press, Taylor and Francis Group, Boca Raton, 2011), 10.1201/b10712.

[38] U. Boscain, M. Sigalotti, and D. Sugny, Introduction to the Pontryagin maximum principle for quantum optimal control, PRX Quantum **2**, 030203 (2021).

[39] C. P. Koch, U. Boscain, T. Calarco, G. Dirr, S. Filipp, S. J. Glaser, R. Kosloff, S. Montangero, T. Schulte-Herbrüggen, D. Sugny, and F. K. Wilhelm, Quantum optimal control in quantum technologies. Strategic report on current status, visions and goals for research in Europe, Eur. Phys. J. Quantum Technol. **9**, 19 (2022).

[40] N. Dupont, Control and transport of matter waves in an optical lattice, Ph.D. thesis, Université Toulouse 3—Paul Sabatier, 2022.

[41] M. V. Berry and M. Robnik, Semiclassical level spacings when regular and chaotic orbits coexist, J. Phys. A **17**, 2413 (1984).

[42] O. Bohigas, S. Tomsovic, and D. Ullmo, Manifestations of classical phase space structures in quantum mechanics, Phys. Rep. **223**, 43 (1993).

[43] See Supplemental Material at http://link.aps.org/supplemental/10.1103/PhysRevLett.131.133401 for additional materials on the state mixing mechanism, Floquet spectra and study of ratchet transport for longer modulation times.

[44] B. Bahr and H. J. Korsch, Quantum mechanics on a circle: Husimi phase-space distributions and semiclassical coherent state propagators, J. Phys. A **40**, 3959 (2007).

[45] N. Dupont, F. Arrouas, L. Gabardos, N. Ombredane, J. Billy, B. Peaudecerf, D. Sugny, and D. Guéry-Odelin, Phase-space distributions of Bose–Einstein condensates in an optical lattice: Optimal shaping and reconstruction, New J. Phys. **25**, 013012 (2023).

[46] A. Fortun, C. Cabrera-Gutiérrez, G. Condon, E. Michon, J. Billy, and D. Guéry-Odelin, Direct Tunneling Delay Time Measurement in an Optical Lattice, Phys. Rev. Lett. **117**, 010401 (2016).

[47] C. Cabrera-Gutiérrez, E. Michon, V. Brunaud, T. Kawalec, A. Fortun, M. Arnal, J. Billy, and D. Guéry-Odelin, Robust calibration of an optical-lattice depth based on a phase shift, Phys. Rev. A **97**, 043617 (2018).

[48] Having $\gamma = s(E_L/\hbar\omega)^2$ and $\hbar_{\text{eff}} = 4\pi^2\hbar/m\omega d^2$, $\hbar_{\text{eff}}$ is varied without altering the classical dynamics by adjusting the lattice depth $s = 4\gamma/\hbar_{\text{eff}}^2$.

[49] N. Dupont, G. Chatelain, L. Gabardos, M. Arnal, J. Billy, B. Peaudecerf, D. Sugny, and D. Guéry-Odelin, Quantum state control of a Bose-Einstein condensate in an optical lattice, PRX Quantum **2**, 040303 (2021).

[50] This fidelity figure is set as a convergence condition on the iterative QOC algorithm [49].

[51] D. Schrader, S. Kuhr, W. Alt, M. Müller, V. Gomer, and D. Meschede, An optical conveyor belt for single neutral atoms, Appl. Phys. B **73**, 819 (2001).

[52] S. H. Hauck, G. Alber, and V. M. Stojanović, Single-atom transport in optical conveyor belts: Enhanced shortcuts-to-adiabaticity approach, Phys. Rev. A **104**, 053110 (2021).

[53] T. Klostermann, C. R. Cabrera, H. von Raven, J. F. Wienand, C. Schweizer, I. Bloch, and M. Aidelsburger, Fast long-distance transport of cold cesium atoms, Phys. Rev. A **105**, 043319 (2022).